Model of plasmon excitations in a bundle and a two-dimensional array of nanotubes

Tibab McNeish,* Godfrey Gumbs,† and Antonios Balassis‡

Department of Physics and Astronomy, Hunter College at the City University of New York, 695 Park Avenue, New York, New York 10065, USA

We calculate the plasma excitations in a bundle as well as a two-dimensional (2D) periodic array of aligned parallel multishell nanotubes on a substrate. The carbon nanotubes are oriented perpendicular to the substrate. The model we use for the system is an electron gas confined to the surface of an infinitely long cylinder embedded in a background dielectric medium. Electron tunneling between individual tubules is neglected. We include the Coulomb interaction between electrons on the same tubule and on different tubules for the same nanotube and neighboring nanotubes. We present a self-consistent field theory for the dispersion equation for intrasubband and intersubband plasmon excitations. For both the bundle and 2D array of aligned parallel nanotubes, the dispersion relation of the collective modes is determined by a three-dimensional wave vector with components in the direction of the nanotube axes and in the transverse directions. The dispersion equation is solved numerically for a single-wall nanotube 2D array as well as a bundle, and the plasmon excitation energies are obtained as a function of wave vector. The intertube Coulomb interaction couples plasmons with different angular momenta m in individual nanotubes, lifting the $\pm m$ degeneracy of the single-nanotube modes. This effect is analyzed numerically as a function of the separation between the tubules. We show that the translational symmetry of the lattice is maintained in the plasmon spectrum for the periodic array, and the plasmon energies have a periodic dependence on the transverse wave vector $\mathbf{q}_\perp$. For the bundle, the Coulomb interaction between nanotubes gives rise to optical plasmon excitations.

I. INTRODUCTION

Carbon nanotubes (CNTs) are an allotrope of carbon which have been prepared in various configurations. For example, a one atom thick sheet of graphene rolled up into a seamless cylinder with diameter on the order of a nanometer constitutes a single-wall carbon nanotube (SWNT). The ratio of the length of the resulting nanostructure to the diameter exceeds 10^6. The novel properties of such cylindrical carbon tubules have made them potentially useful in many applications in nanoscience. These include photonics, electronics (electrical circuits), and other areas of materials science (to strengthen polymer materials).[1–6] Their extraordinary strength, unique electrical properties, and their ability to conduct heat efficiently have generated considerable interest among both experimentalists and theoreticians.[7–23] Nanotubes may also be produced by synthesis methods, for instance multiwall nanotubes (MWNTs) which consist of multiple layers of graphene rolled in on themselves to form a cylindrical tube. There are two models which can be used to describe the structures of multiwall nanotubes. In the first model, sheets of graphene are arranged in concentric cylinders, e.g., a SWNT nanotube within a larger SWNT nanotube. In the Parchment model, a single sheet of graphene is rolled in around itself. The interlayer distance in multiwall nanotubes is close to the distance between graphene layers in graphite, approximately 3.3 Å. Double-wall carbon nanotubes (DWNT) are particularly interesting because they combine similar morphology and properties compared to SWNT, but improving significantly their resistance to chemicals.[7,9] It is abundantly clear that carbon nanotubes are unique nanostructures with remarkable mechanical and electronic properties.[1–3] Interest has focused on them as prototypes for one-dimensional quantum wires as well as how these one-dimensional properties would be modified when the nanotubes are combined in a linear array on a two-dimensional (2D) plane or arranged on a three-dimensional lattice. In Fig. 1, we show schematically an array of nanotubes. We show that the system of nanotubes would lead to a coupling between the plasmon modes.

Over the years, there have been a number of experimental measurements[24–27] and theoretical calculations[28–30] dealing with the effects due to coupling between nanotubes. In the work of Taverna *et al.*[24] employing electron energy-loss spectroscopy (EELS), it was demonstrated that due to the
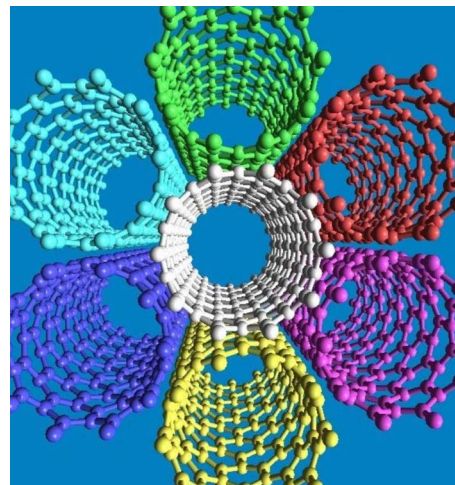

FIG. 1. (Color online) Array of nanotubes whose axes are parallel and taken to be aligned in the *z*-direction. In this paper, we consider a subset forming a bundle, and an infinite periodic array in both *x* and *y*-directions.

strong intratube and intertube Coulomb couplings, there is an in-plane mode and an out-of-plane mode for an array of nanotubes arranged on a two-dimensional surface. This is in agreement with the work of Gumbs and Aĭzin[7] who derived the dispersion equation for nanotubes whose axes are aligned on a planar surface (see also the paper by Shyu and Lin[10]). Stéphan *et al.*[25] reported on a detailed experimental investigation of the plasmon excitations of multiwall carbon nanotubes using EELS. The results in Ref. 25 compared the plasmon modes for MWNTs with those measured for SWNTs. In interpreting their data,[25] a continuum dielectric model was adopted in which the bulk response function for the material making up the nanoparticles was used. The EELS experiments yielded high energy excitations with energies in the 5–15 eV range. Lower energy plasmon excitations (~ 0.5 eV) were measured by Murakami *et al.*[26] in aligned SWNTs on a planar surface forming a thin film by means of optical-absorption techniques, thereby demonstrating the anisotropy of the modes.[7] Films of thickness 1000 Å consisting of SWNTs with mean diameter 4 nm have been probed using EELS and the plasmon mode dispersion was obtained.[27] This means that there are about 25 SWNTs stacked on top of each other; within the limits of the resolution for the momentum and energy transfer for the EELS experiments reported in Ref. 27 (see also the paper by Thess *et al.*[31]). The observed plasmons are in the energy range of 5–7 eV and wave number ~ 0.15 Å^{-1} and are believed to be excitations of the π electrons which are formed by the $2p_z$ orbitals.[19] For metallic and narrow-gap semiconducting SWNTs, the plasmon excitation energies are of low frequency with energies in the range <1 eV.[19] These collective excitations are due principally to the excitation of the charge carriers in the low-energy bands near the Fermi level. With higher spectroscopic resolution, these low-frequency plasmon excitations should be observed, as we demonstrate in this paper with the use of a simple model which is valid for this range of frequencies. The results for the low-frequency plasmon excitations in the tight-binding approximation agree with the electron-gas model for SWNTs and DWNTs (see Refs. 19 and 29 as well as references therein) and this is the reason we use the present model for an array.

The electron-gas model for metallic carbon nanotube bundle was presented by Lin *et al.*[28] following the reported experiments of Thess *et al.*[31] Their formalism for calculating the dispersion equation for this three-dimensional electron system was based on the RPA. However, since the plasmon excitations cannot be categorized as intrasubband and intersubband plasmons as for a single tubule, it is crucial to include the coupling between subbands with different angular-momentum quantum numbers. It is the purpose of this paper to calculate the dispersion relation of the low-frequency plasmons for doped[32] nanotubes in which the charge carriers are introduced onto the graphene tubules by means of intercalation, as can be done in carbon fibers or C_{60}.[33] Also, we investigate the way in which this dispersion relation is affected by their geometrical arrangement, such as their separation and angular configuration. This effect may be analyzed through the behavior of the collective plasma excitations. We do so by calculating numerically the plasma dispersion as a function of the separation between the tubules. We demonstrate that for a bulk lattice the translational symmetry of the lattice is maintained in the plasmon spectrum, and the plasmon energies have a periodic dependence on the transverse wave vector components.

We first calculate the plasmon dispersion equation for an isosceles right triangle of nanotubes as a simple example of a bundle of nanotubes on a substrate with their axes aligned parallel to the z-axis.[34–39] The weak van der Waals interaction which holds them together is neglected in our calculations. The carbon nanotubes are oriented perpendicular to the substrate. With one of the axes of the tubules on the z-axis, the other tubules have their axes at $x=a_x$ on the x-axis and $y=a_y$ on the y-axis. In the limit $a_x \to \infty$ or $a_y \to \infty$, our dispersion equation reduces to that for a pair of multishell nanotubes, as obtained previously.[23] We examine how the Coulomb interaction effects on the plasmon spectrum depend on the axial separation. In order to consider the role played by the periodicity of a lattice on the collective modes, we consider an array of nanotubes, with their axes parallel to the z axis and equally spaced by distance a_x in the x-direction and a_y in the y-direction. Each nanotube may consist of $M \geq 1$ coaxial cylindrical tubules. We assume that there are no electrons tunneling between the tubules in each nanotube and between the nanotubes. The plasmons are determined by the angular-momentum quantum number m corresponding to transitions within a subband ($m=0$) or between different subbands ($m \neq 0$), as well as the wave vector q_z along the axis of the nanotube and the transverse wave vector components q_x and q_y.

Even in the absence of tunneling, for finite a_x and a_y, the plasmon spectrum for one nanotube is modified by the Coulomb interaction between the nanotubes.[7] Furthermore, the intertubule Coulomb interaction causes the angular momentum not to be conserved in a nanotube array or bundle, and modes with different m are coupled to one another. In particular, the degeneracy of the modes with angular-momentum quantum numbers m and $-m$ is lifted by the Coulomb interaction.

The numerical calculations we present were carried out to analyze the way in which mode coupling modifies the plasmon spectrum. For the bundle consisting of three nanotubes whose axes are at the vertices of a triangle, we calculate the dispersion relation as a function of the transverse and longitudinal components of the wave vector. For the array of nanotubes on a 2D lattice, we show that the symmetry of the lattice is maintained in the plasmon spectrum, and the plasmon excitations depend on the wave vectors q_x and q_y with periods $2\pi/a_x$ and $2\pi/a_y$ in the x and y-directions, respectively. Numerical results are presented for the array of nanotubes on a 2D lattice with $M=1$. We obtain data for the plasmon excitation energies as functions of q_z, q_x, and the lattice period a_x. Different plasmon modes associated with the intrasubband and intersubband electron transitions in the tubules are considered and compared with the results for a single nanotube and a linear array on a 2D planar sheet.

The outline of the rest of this paper is as follows: In Sec. II, we derive the dispersion relation for plasmons in a bundle of nanotubes In Sec. III, we present and discuss the plasma dispersion equation for a periodic array of nanotubes consisting of an arbitrary number of concentric tubules. In Sec. IV,

we present numerical results for the plasmon excitation energies and discuss their properties as functions of their wave vectors and the separation of the nanotubes. We give a summary in Sec. V.

II. THEORETICAL FORMALISM FOR A BUNDLE OF TUBULES

We first consider a simple model of bulk quantities of nanotubes. For this we have a coupled triad of infinitesimally thin nanotubules, with their axes aligned in the z-direction. The nanotubes are predicted to be semiconducting or metallic depending on the chirality of the tubules. The axis of one of the tubules of radius R_1 is located at the origin at $x=0$ and the remaining two tubules each of radius R_2 and R_3 are located at a distance of $x=a_x$ and $y=a_y$ from the origin on the x and y axis, respectively. We shall impose the condition that $a_x > R_1 + R_2$ and $a_y > R_1 + R_3$. There is no tunneling between the tubules so that the eigenfunctions of an electron on the jth tubule $(j=1,2)$ on the x axis or y axis, with axial wave vector and angular-momentum quantum numbers are given by

$$|\nu,j\rangle_x = \frac{e^{ik_z z}}{\sqrt{L_z}} \Psi_{l,j}(\boldsymbol{\rho} - (j-1)a_x \hat{\mathbf{e}}_x),$$

$$|\nu,j\rangle_y = \frac{e^{ik_z z}}{\sqrt{L_z}} \Psi_{l,j}(\boldsymbol{\rho} - (i-1)a_y \hat{\mathbf{e}}_y), \qquad (1)$$

where $\nu = \{k_z, l\}$ and

$$\Psi_{l,j}(\boldsymbol{\rho}) = \frac{e^{il\phi}}{\sqrt{2\pi}} \frac{1}{\sqrt{R_j}} \Phi_j(\rho), \quad \Phi_j^2(\rho) = \delta(\rho - R_j). \qquad (2)$$

The energy eigenvalues are

$$\epsilon_{\nu,j} = \frac{\hbar^2 k_z^2}{2m^*} + \frac{\hbar^2 l^2}{2m^* R_j^2}. \qquad (3)$$

The plasmon dispersion equation can be obtained by solving the density-matrix equation $i\hbar \, d\hat{\rho}/dt = [\hat{H}, \hat{\rho}]$, where $\hat{H} = \hat{H}_0 - e\phi_{\text{ext}}$ and $\hat{\rho} = \hat{\rho}_0 + \delta\hat{\rho}$ with $\langle \nu j | \hat{H}_0 | \nu' j' \rangle = \epsilon_{\nu,j} \delta_{\nu\nu'} \delta_{jj'}$ and $\langle \nu j | \hat{\rho}_0 | \nu' j' \rangle = f_0(\epsilon_{\nu,j}) \delta_{\nu\nu'} \delta_{jj'}$, where $f_0(\epsilon_{\nu,j})$ is the Fermi-Dirac distribution function. In the lowest order of perturbation theory, we obtain

$$\langle \nu j | \delta\hat{\rho}_0 | \nu' j' \rangle = 2e \frac{f_0(\epsilon_{\nu,j}) - f_0(\epsilon_{\nu,j})}{\hbar\omega - \epsilon_{\nu,j} + \epsilon_{\nu,j}} \langle \nu j | \phi_{\text{tot}}(\mathbf{r},\omega) | \nu' j' \rangle. \qquad (4)$$

Here, $\phi_{\text{tot}}(\mathbf{r},\omega) = \phi_{\text{ind}}(\mathbf{r},\omega) + \phi_{\text{ext}}(\mathbf{r},\omega)$ is the sum of the external and induced potentials with $\phi_{\text{ind}}(\mathbf{r},\omega)$ a solution of Poisson's equation

$$\nabla^2 \phi_{\text{ind}}(\mathbf{r},\omega) = \frac{4\pi e}{\epsilon_s} \delta n_{\text{ind}}(\mathbf{r},\omega). \qquad (5)$$

Now, we obtain the following matrix elements for the tubules of radii R_1, R_2 and R_3, i.e.,

$$\langle \nu,j | e^{i\mathbf{q}\cdot\mathbf{r}} | \nu',j' \rangle = \delta_{k_z', k_z - q_z} e^{-im\lambda} i^m J_m(q_\perp R_j) \delta_{jj'}, \qquad (6)$$

where $q_\perp = \sqrt{q_x^2 + q_y^2}$. This yields

$$\delta n_{\text{ind}}(\mathbf{r},\omega)$$

$$= \frac{2e}{V} \sum_{j,j'} \sum_{\nu,\nu'} \frac{f_0(\epsilon_{\nu,j}) - f_0(\epsilon_{\nu',j'})}{\hbar\omega - \epsilon_{\nu,j} + \epsilon_{\nu',j'}} \sum_{\mathbf{q},\mathbf{q}'} \langle \nu',j' | e^{-i\mathbf{q}\cdot\mathbf{r}} | \nu,j \rangle \phi_{\text{ind}}$$

$$\times (\mathbf{q},\omega) \langle \nu,j | e^{i\mathbf{q}'\cdot\mathbf{r}} | \nu',j' \rangle \qquad (7)$$

and

$$\delta n_{\text{ind}}(\mathbf{q},\omega) = \frac{2e}{V} \sum_{k_z} \frac{f_0(\epsilon_{k_z,l;1}) - f_0(\epsilon_{k_z - q_z, l-m;1})}{\hbar\omega - \epsilon_{k_z,l;1} + \epsilon_{k_z - q_z, l-m;1}} e^{-im\vartheta_1} J_m(q_\perp R_1)$$

$$\times \sum_{q_x',q_y'} \phi_{\text{ind}}(q_x',q_y',q_z;\omega) J_m(q_\perp' R_1) \left(\frac{q_x' - iq_y'}{q_\perp'} \right)^m + \frac{2e}{V} \sum_{k_z} \frac{f_0(\epsilon_{k_z,l;2}) - f_0(\epsilon_{k_z - q_z, l-m;2})}{\hbar\omega - \epsilon_{k_z,l;2} + \epsilon_{k_z - q_z, l-m;2}} F_1(m,q_\perp,\vartheta_2;R_2)$$

$$\times \sum_{q_x',q_y'} \phi_{\text{ind}}(q_x',q_y',q_z;\omega) e^{-iq_x' a_x} F_1(m,q_\perp',\vartheta_2;R_2) + \frac{2e}{V} \sum_{k_z} \frac{f_0(\epsilon_{k_z,l;2}) - f_0(\epsilon_{k_z - q_z, l-m;2})}{\hbar\omega - \epsilon_{k_z,l;2} + \epsilon_{k_z - q_z, l-m;2}} e^{-iq_y a_y} F_2(m,q_\perp,\vartheta_3;R_3)$$

$$\times \sum_{q_x',q_y'} \phi_{\text{ind}}(q_x',q_y',q_z;\omega) e^{iq_y' a_y} F_2(m,q_\perp',\vartheta_3;R_3), \qquad (8)$$

where ϑ_2 is the angle between the x-axis and a line drawn from the center of the cylinder at the origin to a point on circumference of the cylinder with its center at $x=a_x$. We also define ϑ_3 as the angle between the y-axis and a line drawn from the center of the cylinder at the origin to a point

on the circumference of the cylinder located on the y-axis at $y=a_y$. In addition, we have introduced the following notation:

$$F_1(m,q_\perp,\vartheta_2;R_2) = e^{-im\vartheta_2} J_m(q_\perp R_2),$$

$$F_2(m,q_\perp,\vartheta_3;R_3) = e^{-im\vartheta_3}J_m(q_\perp R_3). \qquad (9)$$

The potential $\phi_{\text{ind}}(\mathbf{q},\omega)$ in Eq. (7) can be rewritten in terms of $\delta n_{\text{ind}}(\mathbf{q},\omega)$. This gives

$$\delta n_{\text{ind}}(\mathbf{q},\omega) = -\frac{2e^2}{\varepsilon_s}\chi_{1,m}(q_z,\omega)J_m(q_\perp R_1)U_{1,m}(q_z)\left(\frac{q_x+iq_y}{q_\perp}\right)^m$$
$$-\frac{2e^2}{\varepsilon_s}\chi_{2,m}(q_z,\omega)e^{-iq_x a_x}F_1(m,q_\perp,\vartheta_2;R_2)U_{2,m}(q_z)$$
$$-\frac{2e^2}{\varepsilon_s}\chi_{3,m}(q_z,\omega)e^{-iq_y a_y}F_2(m,q_\perp,\vartheta_3;R_3)U_{3,m}(q_z), \qquad (10)$$

with

$$U_{1,m}(q_z) = \frac{1}{L_xL_y}\sum_{q_x,q_y}\frac{\delta n_{\text{ind}}(q_x,q_y,q_z)}{q_x^2+q_y^2+q_z^2}J_m(q_\perp R_1)\left(\frac{q_x-iq_y}{q_\perp}\right)^m,$$

$$U_{2,m}(q_z) = \frac{1}{L_xL_y}\sum_{q_x,q_y}\frac{\delta n_{\text{ind}}(q_x,q_y,q_z)}{q_x^2+q_y^2+q_z^2}e^{iq_x a_x}F_1(m,q_\perp,\vartheta_2;R_2),$$

$$U_{3,m}(q_z) = \frac{1}{L_xL_y}\sum_{q_x,q_y}\frac{\delta n_{\text{ind}}(q_x,q_y,q_z)}{q_x^2+q_y^2+q_z^2}e^{iq_y a_y}F_2(m,q_\perp,\vartheta_3;R_3), \qquad (11)$$

and

$$\chi_{j,m}(q_z,\omega) = 2\sum_{l=-\infty}^{\infty}\int_{-\infty}^{\infty}dk_z\frac{f_0(\epsilon_{k_z,l;j})-f_0(\epsilon_{k_z-q_z,l-m;j})}{\hbar\omega-\epsilon_{k_z,l;j}+\epsilon_{k_z-q_z,l-m;j}}. \qquad (12)$$

After substituting, we obtain

$$U_{1,m}(q_z) = -\frac{2e^2}{\varepsilon_s}\chi_{1,m'}(q_z,\omega)U_{1,m'}(q_z)\frac{1}{L_xL_y}\sum_{q_x',q_y'}\frac{J_{m'}(q_\perp' R_1)J_m(q_\perp' R_1)}{q_x'^2+q_y'^2+q_z^2}\left(\frac{q_x'+iq_y'}{q_\perp'}\right)^{m'-m}$$
$$-\frac{2e^2}{\varepsilon_s}\chi_{2,m}(q_z,\omega)U_{2,m'}(q_z)\frac{1}{L_xL_y}\sum_{q_x',q_y'}e^{-iq_x'a_x}\frac{F_1(m',q_\perp',\vartheta_2,R_2)J_m(q_\perp' R_1)}{q_x'^2+q_z^2}\left(\frac{q_x'+iq_y'}{q_\perp'}\right)^{-m}$$
$$-\frac{2e^2}{\varepsilon_s}\chi_{3,m'}(q_z,\omega)U_{3,m'}(q_z)\frac{1}{L_xL_y}\sum_{q_x',q_y'}e^{-iq_y'a_y}\frac{F_2(m',q_\perp',\vartheta_3,R_3)J_m(q_\perp' R_1)}{q_x'^2+q_z^2}\left(\frac{q_x'+iq_y'}{q_\perp'}\right)^{-m}, \qquad (13)$$

$$U_{2,m}(q_z) = -\frac{2e^2}{\varepsilon_s}\chi_{1,m'}(q_z,\omega)U_{1,m'}(q_z)\frac{1}{L_xL_y}\sum_{q_x',q_y'}e^{iq_x'a_x}\frac{F_1(m,q_\perp',\vartheta_2;R_2)J_{m'}(q_\perp' R_1)}{q_\perp'^2+q_z^2}\left(\frac{q_x'+iq_y'}{q_\perp'}\right)^{m'}$$
$$-\frac{2e^2}{\varepsilon_s}\chi_{2,m'}(q_z,\omega)U_{2,m'}(q_z)\frac{1}{L_xL_y}\sum_{q_x',q_y'}\frac{F_1(m',q_\perp',\vartheta_2,R_2)F_1(m,q_\perp',\vartheta_2,R_2)}{q_\perp'^2+q_z^2}e^{-i(q_x-q_x')a_x}$$
$$-\frac{2e^2}{\varepsilon_s}\chi_{3,m'}(q_z,\omega)U_{3,m'}(q_z)\frac{1}{L_xL_y}\sum_{q_x',q_y'}\frac{F_2(m',q_\perp',\vartheta_3,R_3)F_1(m,q_\perp',\vartheta_2,R_2)}{q_\perp'^2+q_z^2}e^{-iq_y a_y}e^{iq_x'a_x}, \qquad (14)$$

$$U_{3,m}(q_z) = -\frac{2e^2}{\varepsilon_s}\chi_{1,m'}(q_z,\omega)U_{1,m'}(q_z)\frac{1}{L_xL_y}\sum_{q_x',q_y'}e^{iq_y'a_y}\frac{F_2(m,q_\perp',\vartheta_3;R_3)J_{m'}(q_\perp' R_1)}{q_\perp'^2+q_z^2}\left(\frac{q_x'+iq_y'}{q_\perp'}\right)^{m'}$$
$$-\frac{2e^2}{\varepsilon_s}\chi_{2,m'}(q_z,\omega)U_{2,m'}(q_z)\frac{1}{L_xL_y}\sum_{q_x',q_y'}\frac{F_1(m',q_\perp',\vartheta_2,R_2)F_2(m,q_\perp',\vartheta_3,R_3)}{q_\perp'^2+q_z^2}e^{-iq_y a_y}e^{iq_y'a_y}$$
$$-\frac{2e^2}{\varepsilon_s}\chi_{3,m'}(q_z,\omega)U_{3,m'}(q_z)\frac{1}{L_xL_y}\sum_{q_x',q_y'}\frac{F_2(m',q_\perp',\vartheta_3,R_3)F_2(m,q_\perp',\vartheta_3,R_3)}{q_\perp'^2+q_z^2}e^{-iq_y'a_y}e^{iq_y a_y}. \qquad (15)$$

We note that the set of equations in Eqs. (13)–(15) form a simultaneous system in the variables $U_{1,m}(q_z)$, $U_{2,m}(q_z)$, and $U_{3,m}(q_z)$, with $m=0,\pm1,\pm2,\cdots$. These equations may be simplified if we now introduce the following quantities below, i.e., if we set

$$A_{mm'} = \frac{2e^2}{\varepsilon_s}\chi_{1,m'}(q_z,\omega)\frac{1}{L_xL_y}\sum_{q_x',q_y'}\frac{J_{m'}(q_\perp' R_1)J_m(q_\perp' R_1)}{q_\perp'^2+q_z^2}\left(\frac{q_x'+iq_y'}{q_\perp'}\right)^{m'-m},$$

$$B_{mm'} = \frac{2e^2}{\varepsilon_s}\chi_{2,m'}(q_z,\omega)\frac{1}{L_x L_y}\sum_{q'_x,q'_y}e^{-iq'_x a_x}\frac{F_1(m',q'_\perp,\vartheta_2,R_2)J_m(q'_\perp R_1)}{q'^2_\perp + q^2_z}\left(\frac{q'_x + iq'_y}{q'_\perp}\right)^{-m},$$

$$C_{mm'} = \frac{2e^2}{\varepsilon_s}\chi_{3,m'}(q_z,\omega)\frac{1}{L_x L_y}\sum_{q'_x,q'_y}e^{-iq'_y a_y}\frac{F_2(m',q'_\perp,\vartheta_3,R_3)J_{m'}(q'_\perp R_1)}{q'^2_\perp + q^2_z}\left(\frac{q'_x + iq'_y}{q'_\perp}\right)^{-m},$$

$$D_{mm'} = \frac{2e^2}{\varepsilon_s}\chi_{1,m'}(q_z,\omega)\frac{1}{L_x L_y}\sum_{q'_x,q'_y}e^{iq'_x a_x}\frac{F_1(m,q'_\perp,\vartheta_2,R_2)J_{m'}(q'_\perp R_1)}{q'^2_\perp + q^2_z}\left(\frac{q'_x + iq'_y}{q'_\perp}\right)^{m'},$$

$$E_{mm'} = \frac{2e^2}{\varepsilon_s}\chi_{2,m'}(q_z,\omega)\frac{1}{L_x L_y}\sum_{q'_x,q'_y}\frac{F_1(m',q'_\perp,\vartheta_2,R_2)F_1(m,q'_\perp,\vartheta_2,R_2)}{q'^2_\perp + q^2_z}e^{-i(q_x - q'_x)a_x},$$

$$F_{mm'} = \frac{2e^2}{\varepsilon_s}\chi_{3,m'}(q_z,\omega)\frac{1}{L_x L_y}\sum_{q'_x,q'_y}\frac{F_2(m',q'_\perp,\vartheta_3,R_3)F_1(m,q'_\perp,\vartheta_2,R_2)}{q'^2_\perp + q^2_z}e^{-iq_y a_y}e^{iq'_x a_x},$$

$$G_{mm'} = \frac{2e^2}{\varepsilon_s}\chi_{1,m'}(q_z,\omega)\frac{1}{L_x L_y}\sum_{q'_x,q'_y}e^{iq'_y a_y}\frac{F_2(m,q'_\perp,\vartheta_3,R_3)J_{m'}(q'_\perp R_1)}{q'^2_\perp + q^2_z}\left(\frac{q'_x + iq'_y}{q'_\perp}\right)^{m'},$$

$$H_{mm'} = \frac{2e^2}{\varepsilon_s}\chi_{2,m'}(q_z,\omega)\frac{1}{L_x L_y}\sum_{q'_x,q'_y}\frac{F_1(m,q'_\perp,\vartheta_2,R_2)F_2(m,q'_\perp,\vartheta_3,R_3)}{q'^2_\perp + q^2_z}e^{-iq_x a_x}e^{iq'_y a_y},$$

$$I_{mm'} = \frac{2e^2}{\varepsilon_s}\chi_{3,m'}(q_z,\omega)\frac{1}{L_x L_y}\sum_{q'_x,q'_y}\frac{F_2(m',q'_\perp,\vartheta_3,R_3)F_2(m,q'_\perp,\vartheta_3,R_3)}{q'^2_\perp + q^2_z}e^{-iq_y a_y}e^{iq'_y a_y}. \tag{16}$$

We note that F_{mm} and H_{mm} are the only matrix elements containing a product of the two factors $\exp(iq_\perp a_x \cos\vartheta)$ and $\exp(-iq_\perp a_y \sin\vartheta)$. The Jacobi-Auger formula along with a standard formula for $\exp(iz\cos\vartheta)$ and $\exp(\mp i \sin\vartheta)$ produces the above obtained results.

Back substituting the results for the matrix elements in Eq. (16) into Eqs. (13)–(15), respectively, yields the following compact system of simultaneous linear equations

$$U_{1,m} + \sum_{m'}A_{mm'}U_{1,m'} + \sum_{m'}B_{mm'}U_{2,m'} + \sum_{m'}C_{mm'}U_{3,m'} = 0,$$

$$U_{2,m} + \sum_{m'}D_{mm'}U_{1,m'} + \sum_{m'}E_{mm'}U_{2,m'} + \sum_{m'}F_{mm'}U_{3,m'} = 0,$$

$$U_{3,m} + \sum_{m'}G_{mm'}U_{1,m'} + \sum_{m'}H_{mm'}U_{2,m'} + \sum_{m'}I_{mm'}U_{3,m'} = 0. \tag{17}$$

The mode coupling arising from the Coulomb interaction is clearly seen through the finite values of the coefficients when $m' \neq m$ in Eq. (17). The dimension of the associated coefficient matrix above is dependent on the type of transitions being investigated. Therefore, to obtain a matrix of modest dimensions, let us consider only intrasubband transitions (i.e., $m=0$). For such transitions, we have

$$\overleftrightarrow{\epsilon}(\omega,q_x,q_y,q_z)\begin{pmatrix}U_{1,0}(q_z)\\U_{2,0}(q_z)\\U_{3,0}(q_z)\end{pmatrix} \equiv \begin{pmatrix}1+A_{0,0} & B_{0,0} & C_{0,0}\\D_{0,0} & 1+E_{0,0} & F_{0,0}\\G_{0,0} & H_{0,0} & 1+I_{0,0}\end{pmatrix}$$
$$\times\begin{pmatrix}U_{1,0}(q_z)\\U_{2,0}(q_z)\\U_{3,0}(q_z)\end{pmatrix} = \begin{pmatrix}0\\0\\0\end{pmatrix}. \tag{18}$$

For nontrivial solutions of Eq. (18) to exist, one requires that the determinant of the coefficient matrix $\overleftrightarrow{\epsilon}(q_x,q_y,q_z)$ vanish. That is $\mathrm{Det}\,\overleftrightarrow{\epsilon}(q_x,q_y,q_z)=0$. This is the dispersion formula for the plasmons and particle-hole mode intrasubband transitions only. Let us further investigate the intrasubband ($m'=m=0$) plasma dispersion equation. In general, an explicit determination of the elements of the matrix for $m=m'$ leads to a simplification of the results in Eq. (16) and we have

$$A_{mm} = \frac{e^2}{\pi\varepsilon_s}I_m(q_z R_1)K_m(q_z R_1)\chi_{1,m}(q_z,\omega),$$

$$B_{mm} = \frac{e^2}{\pi\varepsilon_s}\chi_{2,m}(q_z,\omega)\int_0^\infty dq_\perp q_\perp \frac{J_0(q_\perp a_x)J_m(q_\perp R_1)J_m(q_\perp R_2)}{q_\perp^2 + q_z^2},$$

$$C_{mm} = \frac{e^2}{\pi\varepsilon_s}\chi_{3,m}(q_z,\omega)\int_0^\infty dq_\perp q_\perp \frac{J_0(q_\perp a_y)J_m(q_\perp R_1)J_m(q_\perp R_3)}{q_\perp^2 + q_z^2},$$

$$D_{mm} = \frac{e^2}{\pi\varepsilon_s}\chi_{1,m}(q_z,\omega)\int_0^\infty dq_\perp q_\perp \frac{J_0(q_\perp a_x)J_m(q_\perp R_1)J_m(q_\perp R_2)}{q_\perp^2 + q_z^2},$$

$$E_{mm} = \frac{e^2}{\pi\varepsilon_s}I_m(q_zR_2)K_m(q_zR_2)\chi_{2,m}(q_z,\omega),$$

$$F_{mm} = \frac{e^2}{\pi\varepsilon_s}\chi_{3,m}(q_z,\omega)\int_0^\infty dq_\perp q_\perp$$
$$\times \sum_{k,k'=-\infty}^{\infty} \frac{i^k J_k(q_\perp a_x)J_{k'}(q_\perp a_y)J_m(q_\perp R_2)J_m(q_\perp R_3)}{q_\perp^2 + q_z^2},$$

$$G_{mm} = \frac{e^2}{\pi\varepsilon_s}\chi_{1,m}(q_z,\omega)\int_0^\infty dq_\perp q_\perp \frac{J_0(q_\perp a_y)J_m(q_\perp R_1)J_m(q_\perp R_3)}{q_\perp^2 + q_z^2},$$

$$H_{mm} = \frac{e^2}{\pi\varepsilon_s}\chi_{2,m}(q_z,\omega)\int_0^\infty dq_\perp q_\perp$$
$$\times \sum_{k,k'=-\infty}^{\infty} \frac{i^k(-1)^{k'} J_k(q_\perp a_x)J_{k'}(q_\perp a_y)J_m(q_\perp R_2)J_m(q_\perp R_3)}{q_\perp^2 + q_z^2},$$

$$I_{mm} = \frac{e^2}{\pi\varepsilon_s}I_m(q_zR_3)K_m(q_zR_3)\chi_{3,m}(q_z,\omega). \tag{19}$$

There is symmetry between the matrix elements appearing in Eq. (19). For example, the only difference between B_{mm} in the first row and second column and D_{mm} in the second row and first column is the susceptibility $\chi_{j,m}(q_z,\omega)$, with $j=1$ or $j=2$. Because of the symmetry under the interchange $R_1 \leftrightarrow R_2$, the form factor in these two matrix elements is the same. Also, the matrix element C_{mm} may be obtained from G_{mm} with the replacement $\chi_{3,m}(q_z,\omega) \rightarrow \chi_{1,m}(q_z,\omega)$ and vice versa. For these two matrix elements, there is symmetry under the interchange $R_1 \leftrightarrow R_3$. Further simplification of these results may be achieved for intrasubband excitation ($m=m'=0$) by means of the identity[40]

$$\int_0^\infty dq_\perp \frac{q_\perp}{q_\perp^2 + q_z^2}J_0(aq_\perp)J_0(bq_\perp)J_0(cq_\perp)$$
$$= I_0(q_za)I_0(q_zc)K_0(q_zb) \quad \text{for} \quad a > b+c; \quad b,c,q_z > 0. \tag{20}$$

In the limit when $a_x \rightarrow \infty$, i.e., when the tubule on the x axis is infinitely far away, the intertubule Coulomb interaction is negligible, and we obtain the following dispersion formula for two tubules on the y axis, i.e.,

$$\text{Det}\begin{pmatrix} 1+A_{0,0} & 0 & C_{0,0} \\ 0 & 1+E_{0,0} & 0 \\ G_{0,0} & 0 & 1+I_{0,0} \end{pmatrix} = 0. \tag{21}$$

In the limit $a_y \rightarrow \infty$, the dispersion equation becomes

$$\text{Det}\begin{pmatrix} 1+A_{0,0} & B_{0,0} & 0 \\ D_{0,0} & 1+E_{0,0} & 0 \\ 0 & 0 & 1+I_{0,0} \end{pmatrix} = 0. \tag{22}$$

Thus, as expected, the dispersion Eqs. (21) and (22) clearly demonstrate a coupling of the modes in a pair of the nanotubes leaving the third isolated from the other two in the bundle. We now turn to a consideration of the dispersion equation for plasma excitations for a 2D array of nanotubes embedded in a background dielectric medium.

III. TWO-DIMENSIONAL ARRAY OF NANOTUBES

Assuming that there is no tunneling between the tubules, the single-particle eigenfunctions for the 2D periodic array are

$$\psi_{j\nu l}(\boldsymbol{\rho},z) = \frac{1}{\sqrt{L_zN_xN_y}}e^{ik_zz}\sum_{n_x=-N_x/2}^{N_x/2}\sum_{n_y=-N_y/2}^{N_y/2}e^{i(k_xn_xa_x+k_yn_ya_y)}\Psi_{jk_zl}$$
$$\times[\boldsymbol{\rho} - (n_xa_x\hat{\mathbf{e}}_x + n_ya_y\hat{\mathbf{e}}_y)],$$

$$\Psi_{jl}(\boldsymbol{\rho}) = \frac{1}{\sqrt{2\pi}}e^{il\phi}\frac{1}{\sqrt{R_j}}\Phi_j(\rho), \tag{23}$$

where $j=1,2,\cdots,M$ labels the tubules in the nanotube, $\nu = \{k_x,k_y,k_z\}$ is a composite index for the electron eigenstates, $\Psi_{jl}(\boldsymbol{\rho})e^{ik_zz}$ is the wave function for an electron in the jth tubule, with wave vector k_z in the axial direction and angular-momentum quantum number $l=0,\pm1,\pm2,\cdots$, $\Phi_i^2(\rho) = \delta(\rho-R_i)$, $k_x = \frac{2\pi}{L_x}n_x$, and $k_y = \frac{2\pi}{L_y}n_y$ with $n_x = 0,\pm1,\pm2,\cdots,\pm\frac{N_x}{2}$ and $n_y = 0,\pm1,\pm2,\cdots,\pm\frac{N_y}{2}$. Here, $N_x = L_x/a_x$ and $N_y = L_y/a_y$ are the numbers of nanotubes in the x and y directions in the array with periodic boundary conditions. Electron motion in the azimuthal direction around the tubule is quantized and characterized by the angular-momentum quantum number l, whereas motion in the axial z direction is free. Thus, the electron spectrum in each tubule consists of one-dimensional (1D) subbands with l serving as a subband index. The spectrum does not depend on k_x and has the form

$$\epsilon_{jk_zl} = \frac{\hbar^2k_z^2}{2m^*} + \frac{\hbar^2l^2}{2m^*R_j^2}. \tag{24}$$

Consequently, using these results in conjunction with the methods previously employed for the one-dimensional array of nanotubes, we obtain the dispersion formula for plasma excitations in a 2D array of nanotubes to be

$$\text{Det}\Bigg[\delta_{mm'}\delta_{jj'}+\frac{2e^2}{a_xa_y\epsilon_s}\chi_{j'm'}(q_z,\omega)\sum_{N_x=-\infty}^{\infty}\sum_{N_y=-\infty}^{\infty}\frac{J_{m'}(R_{j'}\sqrt{(q_x+G_N^x)^2+(q_y+G_N^y)^2})J_m(R_j\sqrt{(q_x+G_N^x)^2+(q_y+G_N^y)^2})}{(q_x+G_N^x)^2+(q_y+G_N^y)^2+q_z^2}$$

$$\times\left(\frac{q_x+G_N^x+i(q_y+G_N^y)}{\sqrt{(q_x+G_N^x)^2+(q_y+G_N^y)^2}}\right)^{m'-m}\Bigg]=0, \tag{25}$$

where $G_N^x=\frac{2\pi N_x}{a_x}$ and $G_N^y=\frac{2\pi N_y}{a_y}$.

The result in Eq. (25) shows that the symmetry of the lattice is maintained in the plasmon spectrum for both the x and y directions. In addition, the plasmon excitations depend on the wave vector components q_x and q_y with periods $2\pi/a_x$ and $2\pi/a_y$. In the limit, $a_y\rightarrow\infty$, we obtain the following dispersion equation for a linear array of nanotubes on a 2D plane, i.e.,

$$\text{Det}\Bigg[\delta_{mm'}\delta_{jj'}+\frac{e^2}{\pi a_x\epsilon_s}\chi_{j'm'}(q_z,\omega)\sum_{N_x=-\infty}^{\infty}\int_{-\infty}^{\infty}dq_y\frac{J_{m'}(\sqrt{(q_x+G_N^x)^2+q_y^2}R_{j'})J_m(\sqrt{(q_x+G_N^x)^2+q_y^2}R_j)}{(q_x+G_N^x)^2+q_y^2+q_z^2}$$

$$\times\left(\frac{q_x+G_N^x+iq_y}{\sqrt{(q_x+G_N^x)^2+q_y^2}}\right)^{m'-m}\Bigg]=0, \tag{26}$$

which agrees with the result obtained by Gumbs and Ašzin.[7]

IV. NUMERICAL RESULTS AND DISCUSSION

We now turn to numerical calculations for an array of nanotubes as well as a bundle based on the formalism we developed in Secs. II and III. We simulate a metallic graphene tubule in a medium with background dielectric constant $\varepsilon_s=2.4$ by choosing $m^*=0.25m_e$, where m_e is the free-electron mass and $E_F=0.6$ eV. The effective Bohr radius is $a_B\equiv\hbar^2\epsilon_s/m^*e^2=1.26$ Å. All calculations were carried out at zero temperature. We included the transitions $m=0,\pm1$ only in the calculations for plasma excitations in a 2D array. The number of occupied subbands in each tubule is determined by its radius, the electron density through the Fermi energy and electron effective mass. The occupied subbands are then included in the sum $l=0,\pm1,\pm2,\cdots,\pm l_{max}$, where l_{max} labels the highest occupied subband at $T=0$ K. For a single wall cylindrical nanotube of radius 11 Å, there are five subbands occupied by electrons corresponding to $l=0,\pm1,\pm2$. Lin and Shung[9] used the same values of ε_s, m^*, R, and E_F in calculating the plasmon excitation spectrum. It was shown that there are three quasiacoustic plasmon branches associated with intrasubband electron excitations with angular-momentum transfer $m=0$. The reason for this is that the plasmon excitations depend on $|l|$ in this case. There are five optical plasmon branches associated with intersubband electron transitions with angular-momentum transfer $m=\pm1$.

In Fig. 2, we present our results for the dispersion relation of intrasubband ($m=0$) plasmon excitations of a 2D array of single wall nanotubes. The radius of each tubule is 11 Å and the period of the lattice is 35 Å. The excitation energy is plotted as a function of q_z with $q_x=\pi/a_x$ and $q_y=\pi/a_y$. Only the plasmon branches which are not Landau damped and which lie outside the single-particle excitation regions are presented in Fig. 2. For the sake of clarity, we have omitted the boundaries of the particle-hole continuum in this figure. In Fig. 3, we plot the intrasubband plasmon energies as a function of $q_xa_x/2\pi$ for fixed q_y and q_z, using the same lattice parameters as Fig. 2. Only the plasmon modes which are not Landau damped by the single-particle excitations are shown in Fig. 3. There are several branches of plasmon excitations in both Figs. 2 and 3. The periodicity of the lattice is preserved in each of the plasmon branches when plotted as functions of the transverse wave vector q_x.

It is a simple matter to show from Eq. (26) that for a 1D array, when $q_x=0$ the elements of the determinantal matrix with $m=0$, $m'=\pm1$ are zero due to antisymmetry of the q_y integrand. This means that there is decoupling of the intrasubband and intersubband excitations. Similarly, it follows from Eq. (25) that when *both* $q_x=0$ and $q_y=0$, the matrix elements of the determinantal equation are zero for $m=0$ and $m'=\pm1$ as well. The main result of these plots is to show that the Coulomb interaction between the tubules in the 2D
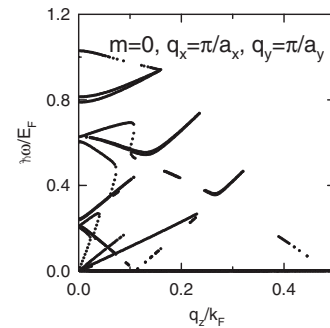

FIG. 2. Undamped intrasubband ($m=0$) plasmon excitation energy, in units of the Fermi energy E_F, as a function of q_z/k_F. Here, k_F is the Fermi wave number in the ground ($l=0$) subband obtained. The solutions were obtained by solving Eq. (25) for $q_x=\pi/a_x$ and $q_y=\pi/a_y$. The parameters used in the calculation are $m^*=0.25m_e$, where m_e is the bare electron mass and $a_x=a_y=35.0$ Å, $R=11.0$ Å, and $E_F=0.6$ eV.
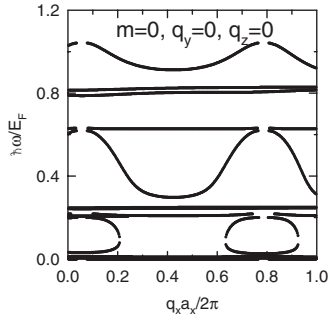
FIG. 3. Undamped intrasubband ($m=0$) plasmon excitation energy as a function of the transverse wave vector q_x (in units of $2\pi/a_x$). The solutions are based on Eq. (25) for $q_y=0$ and $q_z=0$. All other parameters employed in obtaining Fig. 2 are the same.

array serves to alter substantially the dependence of the plasmon frequency on q_z. Furthermore, as the separation between tubules is decreased, the plasmon frequency is increased due to the role played by the Coulomb interaction between the tubules. Some of the plasmon branches in Fig. 3 show a stronger dependence on q_x than others. This variation is more pronounced for the high-frequency plasmon mode compared with some of the lower-lying frequency ones.

The effect of the Coulomb interaction on the intrasubband plasmon excitation spectrum of a 2D array of nanotubes consisting of a pair of coaxial tubules is demonstrated in Fig. 4. The outer radius is $R_1=14.4$ Å and the inner radius is R_2 $=11$ Å. The period of the lattice was chosen as $a_x=a_y$ $=35$ Å in both the x and y directions. Only those branches which are not Landau damped by single-particle excitations are shown in this figure. The two highest modes originate from the high-energy modes of each tubule. The Coulomb interaction between the coaxial tubules leads to optical branches which are not present for a single tubule, all of whose modes are acoustic in nature.

Plasmon excitations arising from intersubband electron transitions for $m=\pm 1$ are in Figs. 5 and 6 for the 1D and 2D periodic arrays of single-wall nanotubes. In both figures, only undamped plasmon modes are shown and the particle-hole continuum is omitted. The highest modes have a stronger dependence on the transverse wave vector q_x than
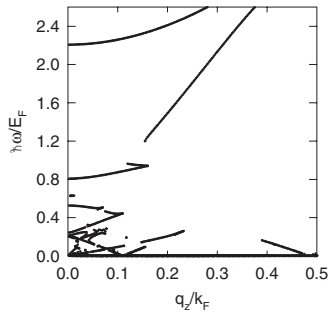

FIG. 4. The plasmon excitation energy, in units of the Fermi energy E_F, as a function of q_z/k_F, for a 2D array of coaxial tubules of outer and inner radii $R_1=14$ Å and $R_2=11$ Å, respectively. The lattice constants in both x and y directions were chosen as 35 Å. The solutions were obtained from Eq. (25), when both $a_x, a_y \rightarrow \infty$. The parameters used in the calculation are the same as in Fig. 2.
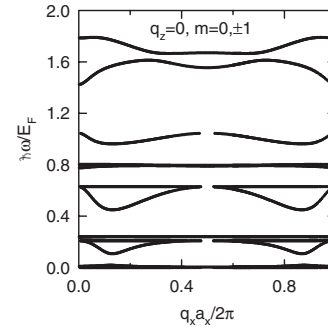

FIG. 5. For a 1D periodic array, the plasmon excitation energy, in units of the Fermi energy E_F, as a function of q_x, in units of $2\pi/a_x$. Here $q_z=0$, the radius of each tubule is 11 Å, and the period is $a_x=35$ Å. All other parameters are the same as in Fig. 2.

the lower modes. This is more so for the 1D array than for the 2D array. The main difference between these intersubband modes in a single tubule compared with a linear 1D array of tubules and when they are arranged in a 2D lattice may be explained in the following way. In a single tubule, plasmon modes with $m=+1$ and -1 are degenerate.[9] The periodic lattice of tubules in either one direction or in two directions removes the axial symmetry of the structure. The Coulomb interaction between the tubules lifts the degeneracy and splits each single tubule intersubband plasmon mode into two branches, increasing the total number of modes to ten for both the 1D and 2D lattices. The Coulomb interaction seems to have a larger effect on the lowest modes for the 1D lattice. Furthermore, this splitting is larger for the high-frequency modes compared with the low-frequency ones. This is demonstrated in Figs. 5 and 6. As a matter of fact, the splitting of the low-frequency modes is too small to be resolved on the scale used in the figures.

Figure 7(a) shows the dispersion relation for intrasubband plasmon excitations obtained by solving for the zeros of the determinant matrix in Eq. (18). The plasmon energy is plotted as a function of the wave vector q_z, for fixed $a_x=a_y$ $=25.0$ Å. The radius of each of the three cylinders is 11 Å. Each of the three cylinders has three plasmon branches when it is not interacting with either one of the two other cylinders. The Coulomb interaction between electrons on different tubules splits the degenerate plasmon modes for each tubule.
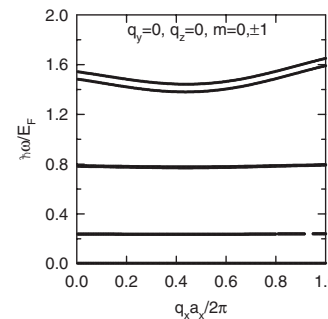

FIG. 6. For a 2D periodic array, the plasmon excitation energy, in units of the Fermi energy E_F, as a function of q_x, in units of $2\pi/a_x$. Here $q_y=q_z=0$; all other parameters are the same as in Fig. 2.
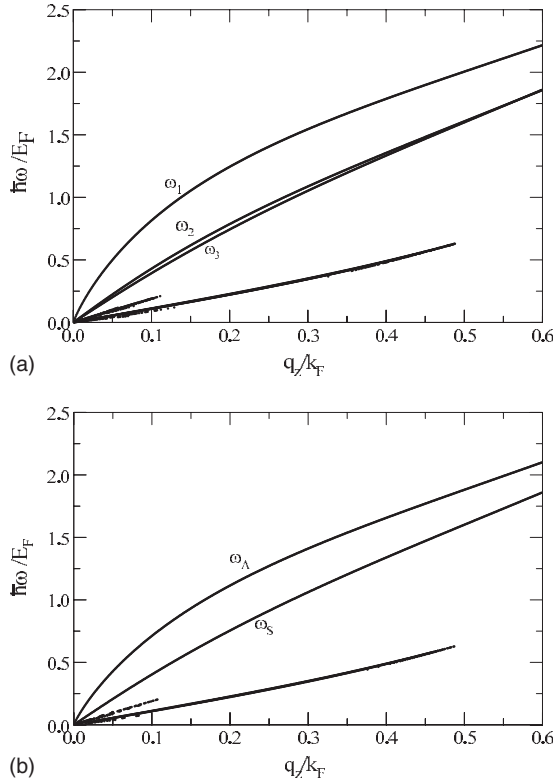
FIG. 7. The intrasubband plasmon excitation energy, in units of the Fermi energy E_F, as a function of q_z/k_F, for the three single wall nanotubes described in Sec. II. The radius of each tubule was chosen as 11 Å and the centers of the tubules are at $a_x=25$ Å and $a_y=25$ Å in (a). In (b), there are only two nanotubes with one fixed at the origin while the position of the second nanotube on the x axis is at $a_x=25$ Å. All other parameters are the same as in Fig. 2.

FIG. 8. The intrasubband plasmon excitation energy, in units of the Fermi energy E_F, as a function of q_z/k_F, for the three single wall nanotubes described in Sec. II. The radius of each tubule was chosen as 11 Å and the separation between the center of the tubules on the y axis is $a_y=25$ Å in (a) while the coordinate of the third tubule on the x axis is varied. In (b), there are two nanotubes with one fixed at the origin while the center of the second one on the x axis is varied. All other parameters are the same as in Fig. 2.

The energy gap between split modes is very much determined by the distance between the tubules. When a_x or a_y increases, the separation between the split modes decreases, reducing to zero as the limits $a_x, a_y \to \infty$. Our numerical analysis shows that the amount by which the branches is split depends on their frequency. To understand the results in Fig. 7(a) better, we plot the dispersion relation for a pair of single wall nanotubes in Fig. 7(b) with $a_x=25$ Å and all other parameters are the same as in Fig. 7(a). The two highest modes in Fig. 7(b) are symmetric (ω_S) and antisymmetric (ω_A) modes. When the third nanotube is introduced in Fig. 7(a), a third high-frequency mode appears (ω_1, ω_2, and ω_3). Since the nanotube with its center located at $x=a_x$ is not separated by the same distance from the nanotube with its center at the origin and the nanotube with its center at $y=a_y$, the plasmon modes ω_1, ω_2, and ω_3 are not equally spaced. There is a total of nine plasmon modes in Fig. 7(a) and six plasmon modes in Fig. 7(b), but not all of them could be seen in these plots. In Figs. 8(a) and 8(b), we fixed the value of the longitudinal wave vector at $q_z=0.2k_F$ and plotted the intrasubband plasmon excitation energies as functions of a_x. Figure 8(a) was obtained for three nanotubes with $a_y=25$ Å, whereas, Fig. 8(b) was calculated for two nanotubes on the x axis with one of them fixed at the origin. The radius of each of the nanotubes was chosen as 11 Å and all other parameters are the same as in Figs. 7(a) and 7(b). The highest plasmon modes
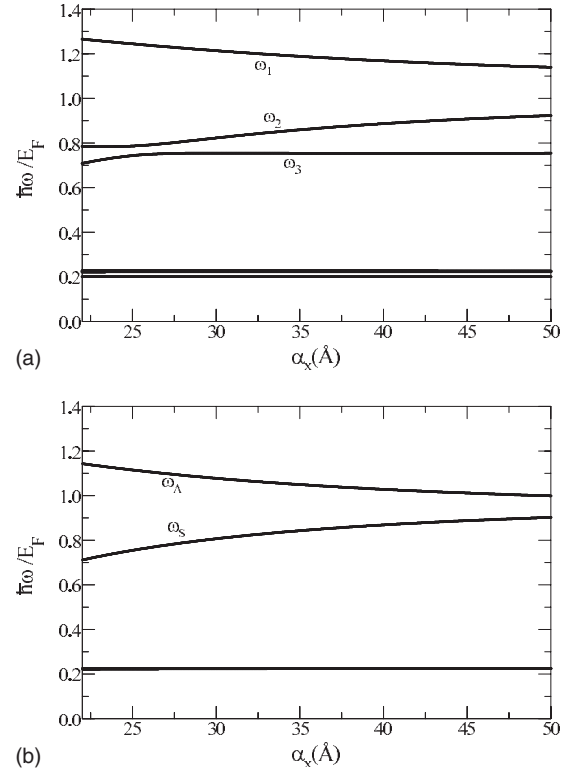
are degenerate in the limit $a_x \to \infty$ in Fig. 8(b) for the pair of nanotubes. The ω_1 and ω_2 modes become degenerate as $a_x \to \infty$. The ω_3 mode splits off from these two modes when the a_x coordinate is large due to the finite Coulomb interaction between the nanotubes on the y axis. As a matter of fact, the ω_3 branch is flat for large a_x since the Coulomb interaction between nanotubes is not affected in this limit. The low-frequency branches shown in Figs. 8(a) and 8(b) clearly have a weak dependence on the variation of the Coulomb interaction with a_x. When $a_x \approx 25$ Å, the ω_2 and ω_3 modes anti-cross, indicating that beyond this distance the Coulomb interaction is strongest between the two nanotubes on the y axis. In general, as shown in Eq. (17), the modes with $m=0$ and $m \neq 0$ are coupled to each other. To illustrate the way in which the Coulomb interaction modifies the plasmon modes for the three tubules, we only present results for $m=0$. In a strict sense, the plasmon excitations cannot be categorized as intrasubband and intersubband plasmons as for a single tubule.

V. SUMMARY

In concluding this paper, we would like to point out that we used a simple electron-gas model to obtain the low-

frequency plasmon excitation spectrum of a 2D periodic array of parallel nanotubes and a bundle of three nanotubes. The nanotubes are assumed doped[32] in which the charge carriers are introduced onto the graphene tubules by means of intercalation, which can be done in carbon fibers or C_{60}.[33] Each nanotube consists of coaxial cylindrical tubules. The starting point of these calculations was to model the electronic band structure of the tubules by a quasi-free-electron gas confined to the surface of an infinitely long cylinder of finite radius. There was no tunneling of electrons between tubules. The random-phase approximation was employed to calculate the plasmon dispersion equation. Plasmon excitation energies were obtained numerically for a single-wall nanotube array as a function of the wave vector q_z along the nanotube axes, with transverse wave vector q_x. The Coulomb interaction between nanotubes acts to split the single-

nanotube plasmon modes. We also obtained the periodic dependence of the plasmon energies on q_x reflecting the translational symmetry of the lattice. Our calculations should serve as a framework for more elaborate computations using the tight-binding method for the band structure for the higher energy plasmon excitations on nanotubes. In our formalism, we showed that plasmon excitations cannot be labeled by the intrasubband or intersubband angular-momentum quantum numbers due to the Coulomb interaction between charge carriers on different tubules.

*tmcneish@hunter.cuny.edu

†ggumbs@hunter.cuny.edu

‡abalassi@hunter.cuny.edu

[1] W. Z. Li, S. S. Xie, L. X. Qian, B. H. Chang, B. S. Zou, W. Y. Zhou, R. A. Zhao, and G. Wang, Science **274**, 1701 (1996).

[2] Z. F. Ren, Z. P. Huang, J. W. Xu, J. H. Wang, P. Bush, M. P. Siegal, and P. N. Provencio, Science **282**, 1105 (1998).

[3] Jian Ping Lu, Phys. Rev. Lett. **79**, 1297 (1997).

[4] Min-Feng Yu, Bradley S. Files, Sivaram Arepalli, and Rodney S. Ruoff, Phys. Rev. Lett. **84**, 5552 (2000).

[5] Chongwu Zhou, Jing Kong, and Hongjie Dai, Phys. Rev. Lett. **84**, 5604 (2000).

[6] Sara M. C. Vieira, Paul Beecher, Ibraheem Haneef, Florin Udrea, William I. Milne, Manoj A. G. Namboothiry, David L. Carroll, Jonghyurk Park, and Sunglyul Maeng, Appl. Phys. Lett. **91**, 203111 (2007).

[7] Godfrey Gumbs and G. R. Aĭzin, Phys. Rev. B **65**, 195407 (2002).

[8] A. Y. T. Leung, X. Guo, X. Q. He, and S. Kitipornchai, Appl. Phys. Lett. **86**, 083110 (2005).

[9] M. F. Lin and Kenneth W.-K. Shung, Phys. Rev. B **47**, 6617 (1993).

[10] F. L. Shyu and M. F. Lin, Phys. Rev. B **60**, 14434 (1999).

[11] Godfrey Gumbs and Antonios Balassis, Phys. Rev. B **68**, 075405 (2003).

[12] Godfrey Gumbs, Y. Abranyos, and T. McNeish, J. Phys.: Condens. Matter **19**, 106213 (2007).

[13] F. J. Garcia-Vidal, J. M. Pitarke, and J. B. Pendry, Phys. Rev. Lett. **78**, 4289 (1997).

[14] J. M. Pitarke and F. J. Garcia-Vidal, Phys. Rev. B **63**, 073404 (2001).

[15] Godfrey Gumbs and Antonios Balassis, Phys. Rev. B **71**, 235410 (2005).

[16] P. Chen, X. Wu, X. Sun, J. Lin, W. Ji, and K. L. Tan, Phys. Rev. Lett. **82**, 2548 (1999).

[17] M. F. Lin and Kenneth W.-K. Shung, Phys. Rev. B **48**, 5567 (1993).

[18] Godfrey Gumbs, A. Balassis, and P. Fekete, Phys. Rev. B **73**, 075411 (2006).

[19] Y. H. Ho, G. W. Ho, S. C. Chen, J. H. Ho, and M. F. Lin, Phys. Rev. B **76**, 115422 (2007).

[20] D. J. Mowbray, Z. L. Miskovic, and F. O. Goodman, Phys. Rev. B **74**, 195435 (2006).

[21] M. Kociak, L. Henrard, O. Stephan, K. Suenaga, and C. Colliex, Phys. Rev. B **61**, 13936 (2000).

[22] A. Seepujak, U. Bangert, A. J. Harvey, P. M. F. J. Costa, and M. L. H. Green, Phys. Rev. B **74**, 075402 (2006).

[23] A. Balassis, Ph.D. thesis, City University of New York, 2006.

[24] D. Taverna, M. Kociak, V. Charbois, and L. Henrard, Phys. Rev. B **66**, 235419 (2002).

[25] O. Stéphan, D. Taverna, M. Kociak, K. Suenaga, L. Henrard, and C. Colliex, Phys. Rev. B **66**, 155422 (2002).

[26] Y. Murakami, E. Einarsson, T. Edamura, and S. Maruyama, Phys. Rev. Lett. **94**, 087402 (2005).

[27] T. Pichler, M. Knupfer, M. S. Golden, J. Fink, A. Rinzler, and R. E. Smalley, Synth. Met. **103**, 2515 (1999).

[28] M. F. Lin, C. S. Huang, and D. S. Chuu, Solid State Commun. **105**, 161 (1998).

[29] Y. H. Ho, G. W. Ho, T. S. Li, and M. F. Lin, Physica E (Amsterdam) **32**, 569 (2006).

[30] M. F. Lin, D. S. Chuu, C. S. Huang, Y. K. Lin, and K. W.-K. Shung, Phys. Rev. B **53**, 15493 (1996).

[31] Andreas Thess, Roland Lee, Pavel Nikolaev, Hongjie Dai, Pierre Petit, Jerome Robert, Chunhui Xu, Young Hee Lee, Seong Gon Kim, Andrew G. Rinzler, Daniel T. Colbert, Gustavo E. Scuseria, David Tománek, John E. Fischer, and Richard E. Smalley, Science **273**, 483 (1996).

[32] M. F. Lin and F. L. Shyu, Physica B (Amsterdam) **292**, 117 (2000).

[33] Y. Chai, T. Guo, C. Jin, R. E. Haufler, L. P. Felipe Chibante, J. Fure, L. H. Wang, J. M. Alford, and R. E. Smalley, J. Phys. Chem. **95**, 7564 (1991).

[34] U. D. Venkateswaran, A. M. Rao, E. Richter, M. Menon, A. Rinzler, R. E. Smalley, and P. C. Eklund, Phys. Rev. B **59**, 10928 (1999).

[35] Maohul Ge and Klaus Sattler, Appl. Phys. Lett. **64**, 710 (1994).

[36] A. Kis, G. Csányi, J.-P. Salvetat, Thien-Nga Lee, E. Couteau, A. J. Kulik, W. Benoit, J. Brugger, and L. Forró, Nat. Mater. **3**,

153 (2004).

[37] Q. H. Wang, T. D. Corrigan, J. Y. Dai, and R. P. H. Chang, Appl. Phys. Lett. **70**, 3308 (1997).

[38] J.-L. Sauvajol, E. Anglaret, S. Rols, and L. Alvarez, Carbon **40**, 1697 (2002).

[39] P. H. Tan, A. G. Rozhin, T. Hasan, P. Hu, V. Scardaci, W. I. Milne, and A. C. Ferrari, Phys. Rev. Lett. **99**, 137402 (2007).

[40] Yu. A. Brychov, O. I. Marichev, and A. P. Prudnikov, *Special Functions*, Integrals and Series Vol. 2 (Gordon and Breach, New York, 1986), p. 232.